Percolation scaling of $1/f$ noise in single-walled carbon nanotube films

Ashkan Behnam, Gijs Bosman, and Ant Ural*
Department of Electrical and Computer Engineering, University of Florida, Gainesville, Florida 32611, USA
(Received 28 April 2008; revised manuscript received 9 July 2008; published 26 August 2008)

We use Monte Carlo simulations and noise modeling to study the scaling of $1/f$ noise in single-walled carbon nanotube films as a function of device parameters and film resistivity. Despite its relative simplicity, this computational approach provides a general framework for the characterization of $1/f$ noise in nanotube films and explains previous experimental observations. We consider noise sources due to both tube-tube junctions and nanotubes themselves. By comparing the simulation results with the experimental data, we find that the noise generated by tube-tube junctions dominates the total nanotube film $1/f$ noise. Furthermore, we systematically study the effect of device length and film thickness on the $1/f$ noise scaling in nanotube films in order to demonstrate that the simulation results are in good agreement with the available experimental data. Our results further show that the $1/f$ noise amplitude depends strongly on device dimensions, nanotube degree of alignment, and the film resistivity, following a power-law relationship with resistivity near the percolation threshold after properly removing the effect of device dimensions. We also find that the critical exponents associated with the noise-resistivity and noise-device dimension relationships are not universal invariants, but rather depend on the specific parameter that causes the change in the resistivity and $1/f$ noise, and the values of the other device parameters. Since $1/f$ noise is a more sensitive measure of percolation than resistivity, these simulations not only provide important fundamental physical insights into the complex interdependencies associated with percolation transport in nanotube networks and films, but also help us understand and improve the performance of these nanomaterials in potential device applications, such as nanoscale sensors, where noise is an important figure of merit.

DOI: 10.1103/PhysRevB.78.085431 PACS number(s): 72.70.+m, 73.63.Fg, 64.60.ah

I. INTRODUCTION

Single-walled carbon nanotube (CNT) two-dimensional (2D) networks, and three-dimensional (3D) films have attracted significant research attention recently due to the fact that they are transparent, conductive, and flexible, and they have uniform physical and electronic properties since individual variations in nanotube diameter and chirality are ensemble averaged.[1–4] As a result, the reproducibility and reliability problems found in devices based on individual nanotubes are solved, and CNT film based devices can be mass produced in a cost-effective manner. Several promising device applications of CNT films have recently been demonstrated, such as thin film transistors,[5,6] flexible microelectronics,[7,8] optoelectronic devices and sensors,[9–12] and chemical sensors.[13–15]

For some of these applications, such as chemical and optoelectronic sensors, intrinsic signal to noise ratio is undoubtedly one of the most important device figures of merit that determine the detection limit of the device.[13,15] It has been shown that for both single nanotubes (regardless of their intrinsic parameters such as diameter and chirality) and CNT films, $1/f$ noise level can be quite high compared to other conventional materials.[16,17] As a result, determining the magnitude of the $1/f$ noise, its sources, and its scaling with various CNT film parameters is crucial not only for understanding the fundamental physics of percolation transport, but also for assessing the potential of CNT films for applications where the device noise is an important figure of merit.[18]

One of the first reports on $1/f$ noise in single-walled carbon nanotube networks and mats[16] observed that the noise obeys the empirical equation

$$\frac{S_I}{I^2} = \frac{A}{f^\beta}, \tag{1}$$

where S_I is the current noise spectral density, I is the current bias, f is the frequency, β is a constant close to 1, and A is the noise amplitude, which is a measure of the $1/f$ noise level.[16,19] Furthermore, the noise amplitude A was reported to be proportional to the device resistance R, namely $A = 10^{-11}R$.[16] Later studies showed that dependence of A on device parameters, such as device length and resistivity, is more complicated than that.[17,20] For example, in CNT networks, the dependence of A on device length L was reported to be $A = 9 \times 10^{-11} R/L^{1.3}$ over a wide range of L; hence the noise amplitude dependence on L is $A \propto L^{-0.3}$ instead of $A \propto L$ implied from a direct proportionality to resistance.[17] The same work also reported a power-law relationship between noise amplitude and resistivity, i.e., $A \propto \rho^{1.6}$ (instead of a linear relationship $A \propto \rho$ predicted from a direct proportionality to resistance) when the application of a gate bias caused the change in resistivity of the CNT network. In a more recent study, $A \propto \rho^{1.3}$ was reported, when the number of deposited CNT film layers (i.e., CNT film thickness) caused the change in the CNT film resistivity.[20]

In order to investigate the physical and geometrical origins of these experimental findings more systematically, simulation and modeling techniques need to be employed. Although there has been recent modeling and simulation work on the electrical and thermal conductivity of CNT networks and films,[21–24] a computational study of $1/f$ noise in CNT films has not been reported previously. Furthermore, a systematic study of the sources of noise and the effects of various device and nanotube parameters on the percolation

scaling of $1/f$ noise in CNT films remains unexplored.

In this paper, we use Monte Carlo simulations to study $1/f$ noise scaling in CNT films as a function of device parameters and film resistivity. Our study focuses on the noise behavior in CNT films at low frequencies and room temperature, where the shot noise and Johnson-Nyquist noise are negligible and $1/f$ noise is the only dominant noise source. We consider noise sources due to both tube-tube junctions and nanotubes themselves. By comparing the simulation results with the experimental data,[17,20] we find that the noise generated by tube-tube junctions dominates the total CNT film $1/f$ noise. We then systematically study the effect of film dimensions, namely device length, device width, and film thickness, and nanotube degree of alignment (an internal device parameter) on the $1/f$ noise scaling in CNT films. Our results show that the noise amplitude depends strongly on device dimensions and on the film resistivity, following a power-law relationship near the percolation threshold. However, when these two dependencies are separated carefully, it becomes clear that the critical exponent associated with the noise-resistivity relationship is not a universal invariant, but rather depends on the device parameter that causes the change in the resistivity and $1/f$ noise. Despite its relative simplicity, our computational approach explains the experimentally observed $1/f$ noise scaling in CNT films and provides a general framework for their noise characterization, which is very important for assessing their suitability for applications with tight noise limitations.

II. COMPUTATIONAL METHOD

Simulation of the noise properties of the single-walled carbon nanotube film was performed by randomly generating the carbon nanotubes in the film using a Monte Carlo process, finding the locations of the tube-tube junctions in the generated film and solving the current continuity equations for these junctions in a matrix format, following a similar approach as explained in detail previously.[21,22]

Briefly, each nanotube in the film is modeled as a "stick" with fixed length l_{CNT}. The position of one end of the nanotube and its direction on a 2D plane are generated randomly. Each nanotube is assigned randomly to be either metallic or semiconducting with the ratio of the semiconducting to metallic nanotubes set to 2:1, as typically observed experimentally.[25] This process is repeated until the desired value for the nanotube density per layer n in the 2D layer is achieved. An example of a 2D nanotube layer produced by this method is shown in Fig. 1(b), where semiconducting and metallic nanotubes are labeled by different colors. The generated network can also be compared to a real atomic force microscope (AFM) image of a nanotube film, which is shown in Fig. 1(a). The model could be improved by using distribution of nanotube lengths; however, that would not change the noise scaling trends and conclusions arrived by using a fixed "effective" length.

After the 2D nanotube layer is generated, locations of the junctions between nanotubes are determined by the simulation code. It has been experimentally observed that nanotubes in a CNT film have random in plane orientations, but

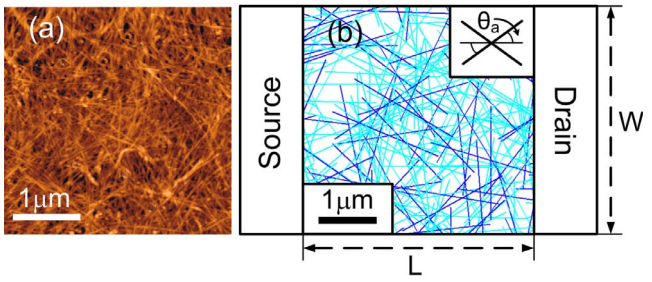

FIG. 1. (Color online) (a) Atomic force microscope (AFM) image of a nanotube film with an approximate thickness of $t=15$ nm where nanotubes are randomly distributed. (b) A 2D nanotube network generated using Monte Carlo simulations for a device with length $L=4$ μm, width $W=4$ μm, nanotube length $l_{CNT}=2$ μm, and nanotube density per layer $n=10$ μm^{-2}. Semiconducting and metallic nanotubes are shown in light and dark color (cyan and blue color online), respectively. The inset illustrates the alignment angle θ_a, which defines the angle range within which nanotubes can be generated to form partially aligned CNT films in simulations.

are mostly ordered to lie in stacked planes.[26] As a result, additional 2D layers are generated randomly using the same approach and stacked vertically to form the 3D nanotube film. In the 3D film, it is assumed that nanotubes in a given layer can also form junctions with nanotubes lying in the first and second nearest-neighbor layers (i.e., two layers above and two layers below), and the locations of these junctions are also determined by the simulation code.

To model the physical properties of the film, the resistance of an individual nanotube is calculated by $R_{CNT}=R_0 l/\lambda$, where l is the length of the nanotube, λ is the mean free path (assumed to be 1 μm in our simulations), and $R_0=h/4e^2$ is the theoretical contact resistance at the ballistic limit ($\sim$6.5 kΩ).[22,27,28] The resistance of the tube-tube junctions depends on whether the junction is metallic/semiconducting (MS), semiconducting/semiconducting (SS), or metallic/metallic (MM).[29] Based on the 2:1 ratio between the semiconducting and metallic nanotubes in the film, about 44% of the junctions are expected to be SS, 44% MS, and 11% MM, which was in perfect agreement with the percentages observed in the simulations. It has been shown that MS junctions have significantly larger contact resistance than MM or SS junctions due to their Schottky nature.[29–31] As a result, we modeled each different type of tube-tube junction by a different contact resistance, instead of a single "effective" contact resistance as done in previous work.[22] In particular, based on previous experimental studies,[29–31] $R_{MM}=25R_0$, $R_{SS}=75R_0$, and $R_{MS}=1000R_0$ were assumed, where R_{MM}, R_{SS}, and R_{MS} are the contact resistances for MM, SS, and MS junctions, respectively.

After the physical properties of the film are defined, a voltage is applied between the source and drain electrodes [see Fig. 1(b)], and the CNT film resistance in the linear regime is calculated by solving a matrix equation based on the application of Kirchoff's current law (KCL) at each junction in the film, as explained in detail previously.[22]

For computing the $1/f$ noise in the CNT film, we have used a model which takes into account the noise contribu-

tions from both the nanotubes themselves and the tube-tube junctions in the film. Assuming independent noise sources (i.e., uncorrelated fluctuations), current-noise spectral density in the film, S_I, can be written as,[32]

$$S_I = \frac{1}{R} \frac{\sum_n i_n^2 s_n r_n^2}{\sum_n i_n^2 r_n}, \tag{2}$$

where i_n is the current, s_n is the current-noise spectral density, and r_n is the resistance of the tube or junction associated with the nth individual noise source, and R is total resistance of the CNT film. Replacing s_n in Eq. (2) by its equivalent based on Eq. (1), S_I can be written as

$$S_I = \frac{1}{Rf} \frac{\sum_n i_n^4 r_n^2 A_n}{\sum_n i_n^2 r_n}, \tag{3}$$

where A_n is the noise amplitude for the nth individual noise source. Finally, an equivalent noise amplitude A_{eq} can be defined for the total CNT film by normalizing Eq. (3), and using $\Sigma_n i_n^2 r_n = I^2 R$ and $V=IR$, where I and V are the total current and voltage in the CNT film, respectively:

$$A_{\text{eq}} = \frac{S_I f}{I^2} = \frac{1}{V^2 I^2} \sum_n i_n^4 r_n^2 A_n, \tag{4}$$

In Eq. (4), all the parameters are known except for the noise amplitudes A_n for individual noise sources.

For individual single-walled carbon nanotubes, it was initially suggested that the noise amplitude scales with nanotube resistance, in other words $A_n \propto R_{\text{CNT}}$.[16] Later studies revealed that the nanotube $1/f$ noise amplitude follows an inverse relationship with the number of carriers N, and hence with the nanotube length l, i.e., $A_n \propto 1/l$.[33] Based on these experimental results, we have used $A_n = 10^{-10} R_0 / l$ for the $1/f$ noise amplitude of individual nanotubes in this work, where l is expressed in microns and $R_0 = 6.5$ kΩ. The chosen coefficient of $10^{-10} R_0$ results in a noise amplitude close to that observed experimentally for individual single-walled carbon nanotubes.[33]

Unlike individual nanotubes, determining A_n for tube-tube junctions based on the available experimental literature is rather difficult. Although the noise in nanotube-based field effect transistors has been studied,[33] there is hardly any experimental data on the noise amplitude of nanotube-nanotube junctions. However, as we will present in the next section, the CNT film noise amplitude observed experimentally and its scaling with device parameters can be fit by our simulations only if we assume that the total CNT film noise is dominated by the tube-tube junctions in the film. The presence of defects or structural deformations[34] at the tube-tube junctions can be speculated as the specific source of this noise, although further experimental studies need to be undertaken to answer this question in depth. In this work, a relationship $A_n = a r_n$ was assumed; in other words, the noise amplitude A_n of an individual tube-tube junction scales linearly with the junction resistance r_n. In all of our simulations, a proportionality constant of $a = 10^{-10}$ was used independent of other device and nanotube parameters, determined from a fit to experimental data. It has been experimentally observed that the $1/f$ noise of a junction between a single one-dimensional (1D) nanotube and a 3D metal source/drain contact could be quite significant, although it does not have to necessarily scale with the contact resistance.[35] Further experimental work is necessary for a detailed understanding of the $1/f$ noise at the junction of two individual nanotubes.

Each data point in the figures represents the average of 500 independent simulations in order to remove the statistical variations in the simulation data calculated from different realizations of the CNT film. Device and nanotube parameters such as film thickness t, nanotube length l_{CNT}, and nanotube density per layer n were chosen to match the experimental values. In addition to matching the $1/f$ noise data, simulations using these parameters, together with the chosen junction and nanotube resistances result in similar CNT film resistivity values to those measured in experiments.[22]

III. RESULTS AND DISCUSSION

Figure 2(a) shows the log-log plot of the noise amplitude normalized to resistance (A/R) versus device length (L) for a single-layer nanotube network, where filled circles denote experimental data points from Snow *et al.*[17] and open circles denote our simulation results. The device and nanotube parameters used in the simulations were device width $W = 2$ μm, nanotube length $l_{\text{CNT}} = 2$ μm, and nanotube density per layer $n = 5$ μm^{-2}, which is within the range of densities reported for thin networks of nanotubes above the percolation limit.[2] Since 2D nanotube networks were used in the experimental work,[17] only a single 2D nanotube layer was used to model the experimental data. The simulation results are in excellent agreement with the experimental data, clearly indicating that A/R is a strong function of device length. The dashed line in Fig. 2(a) is the power-law fit to the experimental data, yielding $A/R \propto L^{\alpha}$ with a critical exponent $\alpha = -1.3$, in agreement with the simulation data for $8 < L < 20$ μm. The deviation of the simulation data from this fit for $L < 8$ μm will be discussed in detail later. This deviation could hardly be noticed in the experiments due to the large scatter in the experimental data points. Simulations here are performed only for $L > 2$ μm because below $L = 2$ μm, individual nanotubes could connect the source and drain electrodes directly (since $l_{\text{CNT}} = 2$ μm), diminishing the effects of percolation. Furthermore, simulations were limited to $L < 20$ μm since the time it takes to run the simulations becomes prohibitively long for longer devices.

The decrease in the noise amplitude with device length is consistent with Hooge's classical empirical law,[36] where the $1/f$ noise amplitude A varies inversely with the number of charge carriers N in the device, i.e., $A \propto 1/N$.[17] However, since the resistance of the CNT film device is given by $R = \rho L / Wt$, where ρ is the resistivity, and N scales with the device volume, i.e., $N \propto LWt$, A/R is expected to scale as $A/R \propto L^{-2}$. Previously, it was suggested that the deviation from this ideal result is due to nonuniformity of the CNT

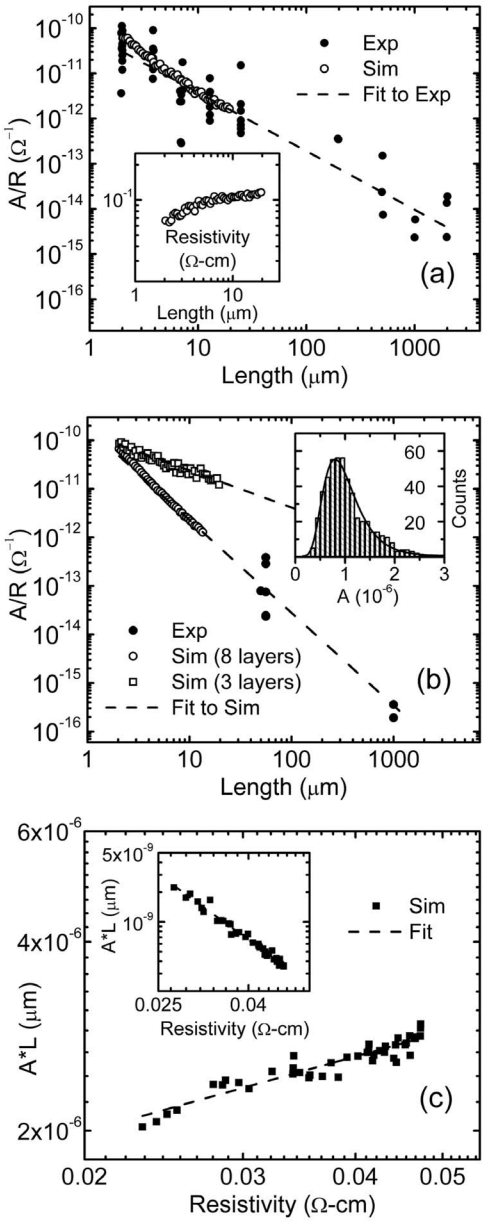

FIG. 2. (a) Log-log plot of the noise amplitude normalized by resistance (A/R) versus device length for a single-layer nanotube network. Experimental data from 2D nanotube networks of Snow *et al.* (Ref. 17) is shown by the filled circles. Our simulation data points for single-layer devices with $W=2$ μm, $l_{CNT}=2$ μm, $n=5$ μm^{-2}, and L ranging from 2 to 20 μm are shown by the open circles. The dashed line fit to the experimental data reported by Snow *et al.* (Ref. 17) has a critical exponent of ~ -1.3, which is same as the exponent obtained from the fit to the simulation data for $8<L<20$ μm. The inset shows log-log resistivity versus device length for the same device as the main panel. Resistivity rolloff is obvious at small device lengths. (b) Log-log plot of noise amplitude normalized by resistance (A/R) versus device length for multilayer nanotube films. Filled circles represent our own experimental measurements (Ref. 37) of CNT film devices with ~ 15 nm thickness, 50 μm and 1000 μm device length, and device widths ranging from 2 to 50 μm. Open circles and squares are our simulation data points for devices with a film thickness of $t=16$ nm (eight layers) and $t=6$ nm (three layers), respectively, where the other simulation parameters are $W=2$ μm, $l_{CNT}=2$ μm, $n=1.25$ μm^{-2}, and L ranging from 2 to 14 μm. The extracted critical exponents from the dashed line fits to these two simulation data sets above $L>6$ μm are −1.9 and −0.8, respectively. The inset shows the distribution of A in 500 simulated devices, all with $L=2$ μm, $t=16$ nm, and the other parameters same as above. The data can be fit by a log-normal distribution as shown. (c) Log-log plot of computed $A\times L$ versus resistivity for the device shown in part (b) with $t=16$ nm. The change in resistivity is a result of the change in device length. The extracted critical exponent of the dashed line fit is 0.4. The inset shows log-log plot of $A\times L$ versus resistivity for the same device as in the main panel, but without any noise sources at the tube-tube junctions. The extracted critical exponent is −2.9 in this case.

network.[17] Our results, on the other hand, suggest that the observed exponent is probably due to the effect of other device parameters on the $1/f$ noise amplitude.

To illustrate this point further, Fig. 2(b) shows how the film thickness t affects the scaling of A/R with L. The simulation parameters are the same as in Fig. 2(a), except that $n=1.25\ \mu\text{m}^{-2}$ (which falls within the range of experimentally reported values for thin nanotube networks[2]) and the number of layers is more than one, which determines the thickness of the simulated CNT film. Two curves are illustrated—one for a film consisting of eight layers ($t\sim 16$ nm, assuming each nanotube layer is 2 nm "thick") and the other for a film consisting of three layers ($t\sim 6$ nm) shown by open circles and squares, respectively. The extracted critical exponents from the power-law fits to the simulation data for $L>6\ \mu$m, shown as dashed lines in Fig. 2(b), are $\alpha=-1.9$ and $\alpha=-0.8$ for the eight- and three-layer CNT film, respectively. As its thickness is reduced, the 3D CNT film becomes like a 2D network and approaches the percolation threshold,[4,26] and the critical exponent α decreases significantly. Furthermore, the magnitude of the critical exponent extracted for the three-layer CNT film is smaller than that for the one-layer 2D network simulated in Fig. 2(a) due to the significantly lower density per layer, n, which is another parameter that affects the critical exponent α. The noise amplitude A also exhibits an inverse power-law dependence on n, decreasing with increasing n. For comparison with the simulation data, our own experimental measurements of the $1/f$ noise amplitude in CNT film devices with $\sim$15 nm thickness, 50 μm and 1000 μm device length, and device widths ranging from 2 to 50 μm are also shown in Fig. 2(b) as filled circles.[37] As can be seen, the simulation results for the $t=16$ nm CNT film are in excellent agreement with the experimental data, and both exhibit a critical exponent which is very close to the ideal case of $\alpha=-2$. In other words, as we get further away from the percolation threshold by changing other device and nanotube parameters, such as increasing the thickness or nanotube density, A/R dependence on L approaches $1/L^2$. In this case, extrapolation of the simulation data to large values of length ($L>20\ \mu$m) is therefore valid, as the CNT film characteristics are similar to a uniform material for large device lengths.

The deviation from this slope observed in the experiments[17] and our simulation data is a clear signature of percolation transport in the CNT film. Furthermore, these results clearly show that the critical exponent α for the device length dependence of A/R is not a universal invariant; rather it depends strongly on other device and nanotube parameters, such as the CNT film thickness and nanotube density. These results illustrate the complex interdependencies that exist for the scaling of the $1/f$ noise in CNT films arising from percolation transport.

Another important point is that there is a significant amount of scatter (about an order of magnitude) in the experimental noise amplitude data from both Snow *et al.*[17] and our own measurements as shown in Figs. 2(a) and 2(b). One of the reasons for this scatter is the percolative nature of the transport in the CNT film. In other words, different physical distribution of nanotubes in the film for devices with the same L can cause the resistivity and noise amplitude to vary significantly. The extent of this scatter is illustrated in the inset of Fig. 2(b) for the $t=16$ nm CNT film simulation data. Here, distribution of the noise amplitude A for 500 different realizations of the CNT film generated randomly is shown for the device length of $L=2\ \mu$m. The simulation data can be fit by a log-normal distribution given by

$$y-y_0=\frac{A}{x\sigma\sqrt{2\pi}}\exp-\frac{\ln(x/x_0)^2}{2\sigma^2}$$

with standard deviation $\sigma\approx 0.4$. This distribution also depends on the other device parameters and becomes wider (i.e., σ becomes larger) as the device dimensions decrease (i.e., as we approach the percolation threshold). For example, it is evident from Fig. 2(b) that there is a large scatter in the noise amplitude simulation data for the three-layer film even after averaging 500 simulation results for each data point. This scatter is absent in the data for the eight-layer thick film. In experimental noise measurements, in addition to this "intrinsic" scatter due to percolation, there are also experimental errors due to factors such as CNT film inhomogeneities and presence of defects and impurities. As a result, the observed variation of an order of magnitude in the experimental noise data can be expected.

As mentioned before, it can be seen in both Figs. 2(a) and 2(b) that the simulation data starts to increase from the dashed line fits for small values of L. This increase is a result of the change in the resistivity ρ of the CNT film. As the device length approaches the length of individual nanotubes (l_{CNT}), the statistical distribution of nanotubes in the film can result in short conduction paths consisting of only a few nanotubes connecting source to drain, decreasing the total resistivity of the film.[21,22] The simulation plot of resistivity versus device length shown in the inset of Fig. 2(a) for the simulation data set in the main panel of Fig. 2(a) illustrates this point. As can be seen, while resistivity decrease with decreasing device length is quite significant for $L<8\ \mu$m, its variation is less than 10% for $L>8\ \mu$m, and the resistivity almost saturates for $L>10\ \mu$m. For very small device lengths, the decrease in resistivity increases the amount of current in the device for a fixed applied bias (in addition to the increase due to the length shrinkage), which in turn increases the total $1/f$ device noise at a rate faster than that observed for larger device lengths, as implied by Eq. (4). This increase in $1/f$ noise causes the critical exponent α to increase for small values of L as evidenced by the deviation from the dashed power-law fits in Figs. 2(a) and 2(b).

The effect of the change in resistivity at small L (due to percolation) on the noise amplitude A can be illustrated further by replotting the data in Fig. 2(b) for the CNT film with $t=16$ nm as $A\times L$ versus resistivity, as shown in Fig. 2(c). We have seen above that the simulation data for the $t=16$ nm curve in Fig. 2(b) exhibits approximately $A/R\sim L^{-2}$, which indicates that $A\times L$ is a constant if ρ is constant. As a result, by plotting $A\times L$ versus ρ in Fig. 2(c), any explicit dependence of A on L is eliminated, except for an implicit dependence through resistivity, since $\rho=\rho(L)$ as seen in the inset of Fig. 2(a). The simulation data in Fig. 2(c) can be fit by a power-law relationship given by $A\times L\propto\rho^{\beta}$ with

an extracted critical exponent of $\beta=0.4$. Since the resistivity is almost constant for many of the data points, they fall on top of or close to each other in Fig. 2(c); however, the scaling trend can still be observed. This observed power law behavior is in agreement with previous results observed for percolation systems[20,38,39] and is a direct manifestation of percolation affecting the $1/f$ noise in the CNT film.

Up to this point, based on the relative noise amplitudes chosen to fit the experimental data, it is assumed that the tube-tube junctions dominate the $1/f$ noise in the CNT film. In contrast, the inset in Fig. 2(c) shows the log-log plot of $A \times L$ versus resistivity, when nanotubes are assumed to be the only sources of $1/f$ noise in the film (tube-tube junction noise amplitudes are set to zero, i.e., $a=0$). There are two striking differences between the results in the main panel and the inset in Fig. 2(c). First, the noise amplitude A has dropped more than 3 orders of magnitude when we exclude the junction noise. In other words, the noise amplitude chosen for an individual nanotube ($A_n=10^{-10}R_0/l$) based on the experimental results for single tube devices[33] results in a total noise significantly smaller than the experimental values observed for the CNT film. This reduction is expected in our simulations, as the noise amplitudes A_n of the tube-tube junctions are significantly larger than those of the nanotubes themselves due to the larger resistance associated with the junctions. Second, $A \times L$ scaling with resistivity now exhibits a power-law *decrease*, which is in sharp contrast to the power-law increase observed in the main panel of Fig. 2(c) for the simulations that fit the experimental data shown in Fig. 2(b). Furthermore, power-law increase in $1/f$ noise with resistivity is commonly observed for CNT films and other systems when a particular parameter is changed to modify the resistivity close to the percolation threshold.[17,20,38,39] We will later show that our simulations exhibit a similar power-law increase in $1/f$ noise with resistivity when the CNT film thickness is the parameter that causes the change in resistivity and $1/f$ noise, in agreement with experimental data.[20] Taken together, the above results strongly suggest that tube-tube junctions, and not the nanotubes themselves, dominate the overall CNT film $1/f$ noise. This finding is in analogy to previous experimental and theoretical results,[22,26] which show that the resistivity of the CNT film is also dominated by tube-tube junction resistance, and not the nanotube resistance. As long as the electronic mean free path is larger than about 100 nm, the nanotube noise remains negligible compared to the junction noise.

Noise scaling trends with other device parameters also confirm the above results. In particular, we next study the effect of device width. The resistivity scaling with device width close to the percolation threshold has been experimentally observed to be significantly more pronounced than that with device length.[22,26] This point is also evident in the simulation data shown in the inset of Fig. 3(a) for a device with $L=5$ μm, $t=16$ nm, and other parameters kept the same as in Fig. 2(b). (These parameters have been used for the rest of the simulations presented in this paper.) In this inset, for $W \geq 2$ μm, resistivity is almost constant, while at submicron width range, it depends strongly on W. We have also performed simulations to investigate the scaling of $1/f$ noise with device width in the CNT film, which has not been experimentally studied. The main panel of Fig. 3(a) shows $1/f$ noise amplitude versus device width W, in which two regions can be distinguished. For $W \geq 2$ μm, A is inversely proportional to W (the power-law exponent extracted from the dashed line fit to the data is $W^{-1.1}$). This variation is expected since $A \propto 1/N$ and the number of carriers N increases linearly with device width, and the resistivity is constant in this regime, as seen in the inset of Fig. 3(a). However, for $W < 1$ μm, there is a strong power-law relationship between A and W with a critical exponent extracted from the fit equal to -5.6. This shows that the variation of resistivity has a strong effect on the noise in this region. To investigate this variation further, the inset of Fig. 3(b) shows A vs ρ for the same data as in the main panel of Fig. 3(a). As can be seen, presenting the data in this way results in a nonlinear curve and its interpretation becomes difficult since this data includes the effect of both W and ρ on the noise.

Once again, to separate these two dependencies, A can be multiplied by W, which eliminates the explicit dependence of A on W. The main panel of Fig. 3(b) shows the log-log plot

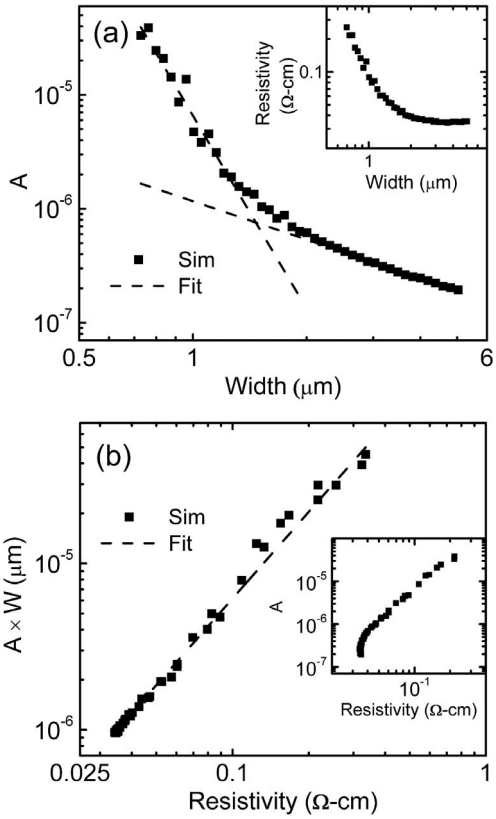

FIG. 3. (a) Log-log plot of computed A versus W for a device with $L=5$ μm, $t=16$ nm, and other parameters same as in Fig. 2(b). There are two separate scaling regimes. The extracted exponent of the dashed line fit for large widths (where resistivity is constant) is -1.1. The extracted exponent of the dashed line fit for small widths is -5.6. The inset shows log-log plot of resistivity versus device width for the same device as in the main panel. (b) Log-log plot of computed $A \times W$ versus resistivity. The change in resistivity is a result of change in device width. The extracted critical exponent in this case is 1.7. The inset shows log-log plot of A versus resistivity for the same device.

of $A \times W$ (noise amplitude normalized with device width) versus resistivity. Similar to the length case, the simulation data can be fit by a power-law dependence on resistivity, $A \times W \propto \rho^{\delta}$, where the extracted critical exponent for width is $\delta = 1.7$. This critical exponent is different from the one extracted for noise scaling with resistivity that was due to the change in device length. This result shows that the noise-resistivity critical exponent is not a universal invariant, rather it depends on the parameter that is causing the change in the $1/f$ noise.

As we have seen in Fig. 2(b), CNT film thickness has a strong effect on the noise scaling with device length. Several studies have shown that film thickness t also has a strong effect on the CNT film resistivity, especially for extremely thin films.[4,26] Recently, Soliveres *et al.* have experimentally studied the dependence of the $1/f$ noise amplitude on film thickness.[20] Next, we investigate this dependence by our simulations. The left inset of Fig. 4(a) shows log-log plot of resistivity versus number of layers (i.e., thickness) where resistivity is almost constant for films with ten layers or more, while strong inverse power-law dependence of resistivity on thickness exists for thin films near the percolation threshold. As a result, like device width, film thickness can be expected to have a strong impact on noise, as shown by the experimental results of Soliveres *et al.*[20] The main panel of Fig. 4(a) shows the log-log plot of the noise amplitude normalized by thickness $A \times t$ versus resistivity computed for the same CNT film device as in the inset. Similar to the width case, the normalized amplitude $A \times t$ is used because A varies with thickness linearly in the regime when resistivity is constant. The simulation data can be fit by $A \times t \propto \rho^{\nu}$, where the extracted critical exponent is $\nu = 1.8$. These results can be compared to the experimental data of Soliveres *et al.*[20] Although they report a critical exponent for A, not $A \times t$, renormalization of their data gives $\nu = 1.1$. The disagreement in the simulation (1.8) and experimental (1.1) critical exponents reported is most likely due to differences between other device/nanotube parameters, such as density per layer, and the film properties such as the purity and homogeneity of the deposited CNT film.

As a confirmation of how the two possible noise sources (nanotube and junction) affect the noise results, the right inset in Fig. 4(a) shows log-log plot of $A \times t$ versus resistivity but with tube-tube junction noise amplitudes set to zero (i.e., nanotube-dominated noise). Similar to the case of device length, not only the noise amplitude A drops by orders of magnitude, the critical exponent also becomes negative, which is in sharp opposition to the positive value observed in experimental data.[20] These results once again imply that the tube-tube junctions dominate the $1/f$ noise in CNT films.

It is worth mentioning that there is slight deviation of the simulation data from the dashed line fit for the highest resistivity value (very thin films) in Fig. 4(a). This is due to the decrease of percolation probability below unity near the percolation threshold,[22] and can be observed for noise scaling with nanotube alignment very close to the percolation threshold as well [Fig. 4(b)].

Finally, we study the effect of alignment of nanotubes making up the film on the scaling of $1/f$ noise amplitude to show that even internal parameters of the film can strongly affect the $1/f$ noise. Nanotube alignment in the film can be quantified by defining a parameter called the alignment angle θ_a, as defined in previous work[40] and illustrated in the inset of Fig. 1(b). Briefly, nanotubes are generated at random angles θ with respect to the horizontal axis, where θ is limited to the range $-\theta_a \leq \theta \leq \theta_a$ and $180 - \theta_a \leq \theta \leq 180 + \theta_a$. As a result, when $\theta_a = 90°$, the nanotubes are completely randomly distributed (which is the case for all the previous simulations), whereas when $\theta_a = 0°$, they are completely aligned along the horizontal axis. Aligned CNT films have been shown to have advantages for applications such as thin film transistors (TFT).[41] The inset in Fig. 4(b) plots resistivity versus nanotube alignment angle obtained by simulations. The resistivity initially decreases, reaches a minimum (at an angle referred to as θ_a^{Min}), and then starts to increase signifi-

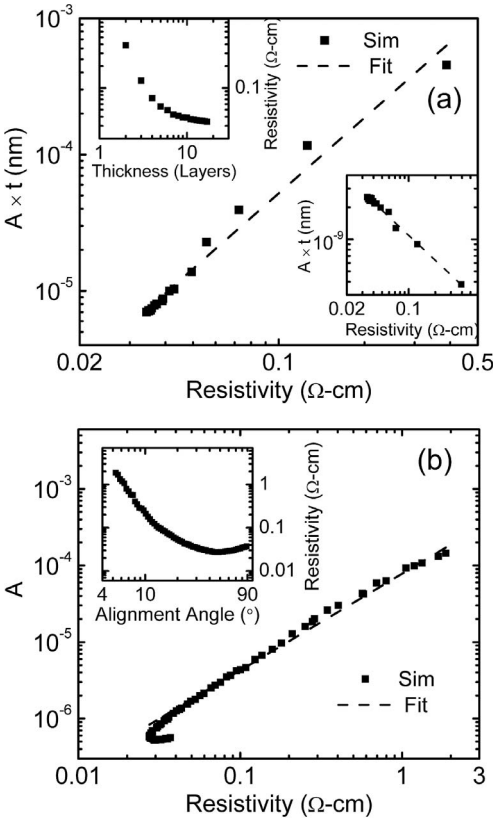

FIG. 4. (a) Log-log plot of computed $A \times t$ versus resistivity. The change in resistivity is a result of change in device thickness. The extracted critical exponent in this case is 1.8. The left inset shows log-log plot of resistivity versus device thickness for the same device. The right inset shows log-log plot of $A \times t$ versus resistivity for the same device, but without any noise sources at the tube-tube junctions. The extracted critical exponent is −0.8 in this case. (b) Log-log plot of computed A versus resistivity. The change in resistivity is a result of change in the nanotube alignment angle θ_a. It is evident that CNT films with the same resistivity values can have two different noise amplitudes, depending on their alignment angles. A power-law fit to the data points (dashed line) with noise amplitudes A higher than 7×10^{-7} yields a critical exponent of 1.3. The inset shows the log-log plot of resistivity versus alignment angle for the same device, in which the resistivity minimum at about 45° is evident.

cantly, as observed experimentally and explained theoretically in detail in previous work.[22,40,42]

The main panel of Fig. 4(b) shows the $1/f$ noise amplitude A versus resistivity, where the high-resistivity section of the curve corresponds to a film with well-aligned nanotubes (i.e., small θ_a). Unlike external device dimensions L, W, and t, the alignment angle θ_a changes device resistance R and noise magnitude A only implicitly by changing ρ and the nature of the conduction paths. As a result, A is not normalized in this figure. Interestingly, it is evident from Fig. 4(b) that CNT films with the same resistivity values can have two different noise amplitudes, depending on their alignment angles. As the alignment angle decreases from 90°, the resistivity becomes smaller, but A remains approximately constant. However, below θ_a^{Min} [about 45° in the inset of Fig. 4(b)], the noise amplitude starts to increase strongly with resistivity. A power-law fit to the noise data with an amplitude higher than 7×10^{-7}, i.e., $A\propto\rho^{\tau}$, yields a critical exponent of $\tau=1.3$. It can be inferred from the trend in Fig. 4(b) that other parameters being constant, partial alignment of nanotubes at the minimum resistivity angle, θ_a^{Min}, gives the lowest resistivity and lowest noise configuration; hence in order to optimize a device design, it is better to have the nanotubes partially aligned in the film rather than perfectly aligned.

IV. CONCLUSIONS

In summary, we have used Monte Carlo simulations and noise modeling to systematically study the $1/f$ noise in CNT films and its scaling with nanotube and device parameters (namely device length, device width, film thickness, and nanotube alignment) and resistivity. We have demonstrated that the Monte-Carlo-based computational noise model can fit previous experimental results on the scaling of $1/f$ noise amplitude in single-walled carbon nanotube films.

Our results show that the $1/f$ noise amplitude depends strongly on device dimensions and on the film resistivity, following a power-law relationship with resistivity near the percolation threshold after properly removing the effect of device dimensions. Furthermore, the noise-resistivity and noise-device dimension critical exponents extracted from the power-law fits are not universal invariants, but rather depend both on the parameter that causes the change in resistivity and noise, and the values of the other device parameters. In addition, the simulation fit to the experimental data strongly suggests that tube-tube junctions, and not the nanotubes themselves, dominate the overall CNT film $1/f$ noise.

The simulations and models presented here are not limited to carbon nanotube films, but are applicable to a broader range of problems involving percolating transport in networks, composites, or films made up of one-dimensional conductors, such as nanowires and nanorods. Since $1/f$ noise is a more sensitive measure of percolation than resistivity, these simulations not only aid experimental measurements by providing important fundamental insights into the physics of percolation transport in nanotube networks and films, but also help understand and improve the performance of these nanomaterials in potential device applications, such as sensors, where noise is an important figure of merit.

ACKNOWLEDGMENTS

This work was funded in part by the University of Florida Research Opportunity Seed Fund and in part by the Semiconductor Research Corporation.

*Author to whom correspondence should be addressed. antural@ufl.edu

[1] Z. Wu, Z. Chen, X. Du, J. Logan, J. Sippel, M. Nikolou, K. Kamaras, J. Reynolds, D. Tanner, A. Hebard, and A. Rinzler, Science **305**, 1273 (2004).
[2] E. S. Snow, J. P. Novak, P. M. Campbell, and D. Park, Appl. Phys. Lett. **82**, 2145 (2003).
[3] Y. X. Zhou, L. B. Hu, and G. Grüner, Appl. Phys. Lett. **88**, 123109 (2006).
[4] E. Bekyarova, M. E. Itkis, N. Cabrera, B. Zhao, A. P. Yu, J. B. Gao, and R. C. Haddon, J. Am. Chem. Soc. **127**, 5990 (2005).
[5] T. Ozel, A. Gaur, J. A. Rogers, and M. Shim, Nano Lett. **5**, 905 (2005).
[6] R. Seidel, A. P. Graham, E. Unger, G. S. Duesberg, M. Liebau, W. Steinhoegl, F. Kreupl, and W. Hoenlein, Nano Lett. **4**, 831 (2004).
[7] K. Bradley, J. C. P. Gabriel, and G. Grüner, Nano Lett. **3**, 1353 (2003).
[8] G. B. Blanchet, S. Subramony, R. K. Bailey, G. D. Jaycox, and C. Nuckolls, Appl. Phys. Lett. **85**, 828 (2004).
[9] C. M. Aguirre, S. Auvray, S. Pigeon, R. Izquierdo, R. Desjardins, and R. Martel, Appl. Phys. Lett. **88**, 183104 (2006).
[10] M. W. Rowell, M. A. Topinka, M. D. McGehee, H. J. Prall, G. Dennler, N. S. Sariciftci, L. Hu, and G. Grüner, Appl. Phys. Lett. **88**, 233506 (2006).
[11] D. Zhang, K. Ryu, X. Liu, E. Polikarpov, J. Ly, M. E. Tompson, and C. Zhou, Nano Lett. **6**, 1880 (2006).
[12] S. Lu and B. Panchapakesan, Appl. Phys. Lett. **88**, 253107 (2006).
[13] G. Esen, M. S. Fuhrer, M. Ishigami, and E. D. Williams, Appl. Phys. Lett. **90**, 123510 (2007).
[14] L. Valentini, I. Armentano, J. M. Kenny, C. Cantalini, L. Lozzi, and S. Santucci, Appl. Phys. Lett. **82**, 961 (2003).
[15] E. S. Snow, F. K. Perkins, E. J. Houser, S. C. Badescu, and T. L. Reinecke, Science **307**, 1942 (2005).
[16] P. G. Collins, M. S. Fuhrer, and A. Zettl, Appl. Phys. Lett. **76**, 894 (2000).
[17] E. S. Snow, J. P. Novak, M. D. Lay, and F. K. Perkins, Appl. Phys. Lett. **85**, 4172 (2004).
[18] D. Tobias, M. Ishigami, A. Tselev, P. Barbara, E. D. Williams, C. J. Lobb, and M. S. Fuhrer, Phys. Rev. B **77**, 033407 (2008).
[19] S. Reza, Q. T. Huynh, G. Bosman, J. S. Oakley, and A. G. Rinzler, J. Appl. Phys. **100**, 094318 (2006).
[20] S. Soliveres, J. Gyani, C. Delseny, A. Hoffmann, and F. Pascal,

Appl. Phys. Lett. **90**, 082107 (2007).
[21] S. Kumar, J. Y. Murthy, and M. A. Alam, Phys. Rev. Lett. **95**, 066802 (2005).
[22] A. Behnam and A. Ural, Phys. Rev. B **75**, 125432 (2007).
[23] S. Kumar, M. A. Alam, and J. Y. Murthy, Appl. Phys. Lett. **90**, 104105 (2007).
[24] C. Kocabas, N. Pimparkar, O. Yesilyurt, S. J. Kang, M. A. Alam, and J. A. Rogers, Nano Lett. **7**, 1195 (2007).
[25] A. Ugawa, A. G. Rinzler, and D. B. Tanner, Phys. Rev. B **60**, R11305 (1999).
[26] A. Behnam, L. Noriega, Y. Choi, Z. Wu, A. G. Rinzler, and A. Ural, Appl. Phys. Lett. **89**, 093107 (2006).
[27] S. Li, Z. Yu, C. Rutherglen, and P. J. Burke, Nano Lett. **4**, 2003 (2004).
[28] J.-Y. Park, S. Rosenblatt, Y. Yaish, V. Sazonova, H. Ustunel, S. Braig, T. A. Arias, P. W. Brouwer, and P. L. McEuen, Nano Lett. **4**, 517 (2004).
[29] M. S. Fuhrer, J. Nygard, L. Shioh, M. Forero, Y. G. Yoon, M. S. C. Mazzoni, H. J. Choi, J. Ihm, S. G. Louie, A. Zettl, and P. L. McEuen, Science **288**, 494 (2000).
[30] P. W. Chiu and S. Roth, Appl. Phys. Lett. **91**, 102109 (2007).
[31] Z. Yao, H. W. Ch. Postma, L. Balents, and C. Dekker, Nature (London) **402**, 273 (1999).
[32] A. A. Snarskii, A. E. Morozovsky, A. Kolek, and A. Kusy, Phys. Rev. E **53**, 5596 (1996).
[33] Y. M. Lin, J. Appenzeller, J. Knoch, Z. Chen, and P. Avouris, Nano Lett. **6**, 930 (2006).
[34] A. Nojeh, G. W. Lakatos, S. Peng, K. Cho, and R. F. W. Pease, Nano Lett. **3**, 1187 (2003).
[35] J. Appenzeller, Y. M. Lin, J. Knoch, Z. Chen, and P. Avouris, IEEE Trans. Nanotechnol. **6**, 368 (2007).
[36] F. N. Hooge, Phys. Lett. A **A29**, 139 (1969).
[37] A. Behnam, M. Kang, Z. Wu, A. G. Rinzler, G. Bosman, and A. Ural (unpublished).
[38] A. J. Breeze, S. A. Carter, G. B. Alers, and M. B. Heaney, Appl. Phys. Lett. **76**, 592 (2000).
[39] J. Planes and A. Francois, Phys. Rev. B **70**, 184203 (2004).
[40] A. Behnam, J. Guo, and A. Ural, J. Appl. Phys. **102**, 044313 (2007).
[41] S. J. Kang, C. Kocabas, T. Ozel, M. Shim, N. Pimparkar, M. A. Alam, S. V. Rotkin, and J. A. Rogers, Nat. Nanotechnol. **2**, 230 (2007).
[42] F. Du, J. Fischer, and K. Winey, Phys. Rev. B **72**, 121404(R) (2005).